magnetochemistry

MDPI

Article

Triggering of Valence Tautomeric Transitions in Dioxolene-Based Cobalt Complexes Influenced by Ligand Substituents, Co-ligands, and Anions

Sriram Sundaresan, Marcel Diehl, Luca M. Carrella and Eva Rentschler *

Department Chemie, Johannes-Gutenberg-Universität Mainz, Duesbergweg 10–14, 55128 Mainz, Germany
* Correspondence: rentschler@uni-mainz.de; Tel.: +49-6131-3925491

Abstract: We report the multistep synthesis of the 1,1′-(piperazine-1,4-diyl)bis(N,N-bis(pyridin-2-ylmethyl)methanamine)(**L^{tpbap}**) octadentate ligand, which, in combination with the known 3,5-di-tert-butylcatechol (**3,5-dbcat**), allowed the preparation of two di-nuclear cobalt complexes [Co_2(**L^{tpbap}**)(**3,5-dbcat**)$_2$](SO_4)·5.5MeOH·2H_2O (**3a**) and [Co_2(**L^{tpbap}**)(**3,5-dbcat**)$_2$](ClO_4)$_2$·1.5H_2O (**3b**). We also report the synthesis of two mono-nuclear cobalt complexes [Co(**3,5-dbsq**)(**3,5-dbcat**)(4-Mepip)$_2$] (**1**) with 4-Mepip being 4-methylpiperidine and (Hpip)[Co(**tbcat**)$_2$(pip)$_2$]·CH_3CN (**2**) where Hpip denotes a piperidinium cation and **tbcat** is the *tetra*-bromocatechol ligand. The obtained complexes were characterized by single-crystal X-ray crystallography, SQUID magnetometry, and IR spectroscopy. The structure of the crystalline material in all the cases was determined at 173 K. The magnetic properties of all complexes were measured between 2 and 380 K. The magnetic data clearly show that mono-nuclear complex **1** and di-nuclear complex **3a** exhibit valence tautomerism with onset around 300 K and 370 K, respectively, whereas the other two complexes **2** and **3b** remain unchanged over the measured temperature range.

Keywords: Valence-Tautomer; cobalt; di-nuclear; di-oxolene

check for updates

Citation: Sundaresan, S.; Diehl, M.; Carrella, L.M.; Rentschler, E. Triggering of Valence Tautomeric Transitions in Dioxolene-Based Cobalt Complexes Influenced by Ligand Substituents, Co-ligands, and Anions. *Magnetochemistry* **2022**, *8*, 109. https://doi.org/10.3390/magnetochemistry8090109

Received: 22 August 2022
Accepted: 15 September 2022
Published: 18 September 2022

1. Introduction

Bistable molecules that are capable of switching the electronic states are recently of a great interest for their potential applications in data storage, sensors, and display devices [1–4]. The most commonly studied spin switchable molecules are the spin-crossover molecules where the transition of the spin state in the metal ion occurs between low spin (LS) state and high spin (HS) state [5–8]. Numerous examples with different metal ions are studied in the literature, including the more common Fe(II) and Fe(III) ions, as well rare examples of Co(II) and even more rare examples of Mn(III) [9–12]. Another less commonly studied class of switchable molecules are Valence Tautomeric (VT) compounds, in which the transition between the two states occurs by an electron transfer within the molecule (intramolecular) between the non-innocent redox-active ligand and the metal ion using an external stimulus, such as temperature, light, and pressure [13–17]. Cobalt complexes coupled with redox-active ligands are excellent candidates to show VT effect and have been studied widely in the literature [13,15–21]. The class of redox active ligands most frequently studied in the literature triggering the VT property are catechol and their derivatives. Di-nuclear cobalt complexes are comparatively less reported than the mono-nuclear ones exhibiting VT [16,22–24]. The effect of the VT transition in solid state is often affected by the lattice solvents, choice of anions, substituents in the ring and crystal packing effects [25–27]. In the present work, we report the synthesis, X-ray structure determination, and magnetic properties of two mono-nuclear and two di-nuclear cobalt complexes. The effect of substituents and the choice of anions in triggering the VT behaviour Is investigated.

2. Materials and Methods

All chemicals including 3,5-di-tert-butylcatechol (**3,5-dbcat**) and *tetra*-bromocatechol (**tbcat**) were used without further purification and were purchased from Alfa Aesar, Acros Organics and Fisher Chemicals. The C, H, and N elemental analyses were carried out on a Foss Heraeus Vario EL (Elementar Analysensysteme GmbH, Langenselbold, Germany) at the microanalytical laboratories of the department of chemistry at the Johannes Gutenberg University Mainz. The infrared absorption spectra were collected at room temperature in a range of 3000–450 cm^{-1} on a Thermo Fischer NICOLET Nexus FT/IR-5700 spectrometer (Thermo Fischer Scientific, Waltham, MA, USA) equipped with Smart Orbit ATR Diamond cell (Thermo Fischer Scientific, Waltham, MA, USA). X-ray diffraction data for the structure analysis were collected from suitable single crystals at 173 K with a STOE IPDS 2T at the Johannes Gutenberg University Mainz. The structures were solved with ShelXT [25,26] and refined with ShelXL [27,28] implemented in the program Olex2 [29]. Magnetic data of a microcrystalline sample were collected using a Quantum Design SQUID magnetometer MPMS-XL in a temperature range between 2 and 380 K with an applied field of 1 kOe (0.1 T). The magnetic contribution from the holder were experimentally determined and subtracted from the measured susceptibility data. The contribution from the underlying diamagnetism was corrected using the Pascals constants [30].

2.1. Ligand Synthesis

2.1.1. N,N′-Bis(cyanomethyl)piperazine

Piperazine (6.45 g, 75 mmol) and chloroacetonitrile (13.59 g, 180 mmol) was dissolved in 300 mL ethanol. To the reaction solution was added sodium carbonate (31.8 g, 300 mmol) in small portions under continuous stirring. The reaction mixture was refluxed overnight. The hot solution was filtered and washed with hot ethanol. The excess solvent was removed, and the filtrate was concentrated under reduced pressure to 120 mL. The yellow solution was cooled at −18 °C to obtain colourless crystalline product after two days which was isolated by filtration in moderate (9.15 g, 55.7 mmol, 74.3%). ^{1}H-NMR (400 MHz, $CDCl_3$)δ (ppm) = 3.57 (s, 4 H, H1), 2.71 (s, 8 H, H7). ^{13}C-NMR (100 MHz, $CDCl_3$) 153. δ (ppm) = 114.3 (s), 51.1 (s), 45.8 (s).

2.1.2. N,N′-Bis(2-aminoethyl)piperazine

N,N′-Bis(cyanomethyl)piperazine (2.50 g, 15.21 mmol) was dissolved in 100 mL THF. A suspension of lithium aluminium hydride (2.66 g, 70.00 mmol) in 100 mL THF was prepared separately. The two solutions were mixed together and refluxed for four hours. The reaction solution was cooled to 0 °C using an ice bath and 2.35 mL water was added dropwise to quench the reaction. In addition to this, 2.35 mL sodium hydroxide solution (15%) and 7.05 mL of water were also added. The reaction suspension was filtered and washed with diethyl ether several times. The filtrate obtained was dried for two hours over sodium sulphate and later the filtrate was evaporated to dryness to obtain the desired product as yellow needles in moderate yields (1.58 g, 9.17 mmol, 60.3%). ^{1}H-NMR (400 MHz, $CDCl_3$) δ (ppm) = 2.71 (t, J = 6.3 Hz, 4 H, H8), 2.41 (s, 4 H, H1), 2.35 (t, J = 6.3 Hz, 4 H, H7), and 1.47 (s, 4 H, H9). ^{13}C-NMR (100 MHz, $CDCl_3$) δ (ppm) = 61.14 (s, C7), 53.24 (s, C1), and 38.78 (s, C8).

2.1.3. 1,1′-(piperazine-1,4-diyl)bis(N,N-bis(pyridin-2-ylmethyl)methanamine)($\mathbf{L^{tpbap}}$)

N,N′-Bis(2-aminoethyl)piperazine (1.05 g, 5.8 mmol) was dissolved in 150 mL dichloro methane. To the reaction mixture was added sodium triacetoxyborohydride (6.15 g, 29.0 mmol) slowly in small portions. The 2-pyridinecarboxaldehyde (2.61 g, 24.4 mmol) was dissolved in 10 mL dichloromethane was added to the reaction mixture slowly dropwise over 30 min. The reaction mixture was stirred for two days in room temperature. To the reaction mixture, 50 mL saturated sodium bicarbonate was added whereupon an immediate evolution of CO_2 gas was seen. The reaction mixture was then stirred for additional 30 min. After which, the desired crude product was obtained by extraction with dichloromethane

and ethyl acetate. The organic phase was collected and dried over sodium sulphate which was evaporated to dryness. The solid was purified by washing with acetone several times to obtain the desired product in high yields as yellow powder which was dried under vacuum for four days (3.01 g, 5.6 mmol, 97%). ^{1}H-NMR (400 MHz, $CDCl_3$) δ (ppm) = 8.57 to 8.44 (m, 4 H, H22), 7.65 (td, 4 H, H24), 7.52 (d, 4 H, H25), 7.15 (ddd, 4 H, H23), 3.85 (s, 8 H, H13), 2.74 (t, 4 H, H9), and 2.67 to 2.22 (m, 16 H, H1,7). ^{13}C-NMR (100 MHz, $CDCl_3$) δ (ppm) = 159.61 (s, C17), 148.97 (s, C22), 136.45 (s, C24), 123.02 (s, C25), 122.00 (s, C23), 60.70 (s, C13), 56.06 (s, C7), 52.98 (s, C9), and 51.22 (s, C1). IR (cm^{-1}) = 3421 (br), 3057 (w), 3009 (w), 2939 (m), 2811 (m), 1589 (s), 1570 (m), 1471 (m), 1431 (s), 1363 (m), 1318 (m), 1301 (m), 1248 (m), 1145 (m), 1124 (m), 1051 (m), 1013 (m), 982 (m), 958 (w), 939 (w), 890 (w), 822 (w), 766 (s), 731 (w), 610 (w), 463 (w), and 410 (w).

2.2. Complex Synthesis

2.2.1. $[Co_2(OH_2)(piv)_4(Hpiv)_4]$ (**P1**)

The precursor complex used for the preparation of the mono-nuclear complexes **1** and **2** was synthesized according to the literature [31]. To a solution of pivalic acid (40.0 g, 392 mmol) in 4 mL water was added cobalt carbonate hydrate (8.0 g, 68.0 mmol). The reaction mixture was refluxed at 100 °C overnight. The reaction mixture was cooled to 80 °C for addition of 100 mL acetonitrile. The reaction mixture immediately changed to dark purple solution. The mixture was kept undisturbed overnight to form dark purple crystalline product in moderate yields (19.8 g, 20.9 mmol, 61.4%).

2.2.2. $[Co(3,5\text{-dbsq})(3,5\text{-dbcat})(4\text{-Mepip})_2]$ (**1**)

To a solution of **P1** (237 mg, 0.25 mmol) and **3,5 dbcat** (333 mg, 1.5 mmol) in 15 mL acetonitrile was added 4-methylpiperidine (298 mg, 3.0 mmol). The reaction mixture was refluxed for an hour. The reaction mixture was cooled to room temperature and was filtered to remove undissolved insoluble residues and was set to slowly evaporate. After a day, the desired complex was collected as brown crystalline needles in high yields (249 mg, 0.36 mmol, 71.4%) which was filtered and washed with cold acetonitrile. Elemental Analysis: Found: C, 68.59; H, 9.45; N, 4.48. Calculated for $C_{40}H_{66}CoN_2O_4$: C, 68.84; H, 9.53; and N, 4.01%. IR (cm^{-1}) = 3567 (br), 2951 (s), 2869 (m), 2360 (w), 1573 (m), 1460 (m), 1415 (m), 1358 (m), 1278 (m), 1243 (m), 1199 (m), 1095 (m), 981 (m), 860 (m), 746 (w), 651(m), 577 (w), 545 (w), 493 (w), and 446 (w).

2.2.3. $(Hpip)[Co(tbcat)_2(pip)_2]CH_3CN$ (**2**)

To a solution of **P1** (237 mg, 0.25 mmol) and **H_2tbcat** (319 mg, 0.75 mmol) in 15 mL acetonitrile was added piperidine 128 mg. The reaction mixture was refluxed for an hour. The reaction mixture was cooled to room temperature and was filtered to remove insoluble residue and was set to slow evaporation. The desired product was obtained in moderate yields as brown crystalline solid (173 mg, 0.14 mmol, 29.8%) which was filtered and washed with cold acetonitrile. Elemental Analysis: Found: C, 29.09; H, 3.01; N, 4.76%. Calculated for $C_{27}H_{34}Br_8CoN_3O_4{\cdot}CH_3CN$: C, 28.93; H, 3.10; and N, 4.65%. IR (cm^{-1}) = 3443 (br), 2936 (w), 2854 (w), 1596 (w), 1432 (s), 1348 (w), 1263 (m),1232 (m), 1085 (w), 1026 (w), 1004 (w), 930 (m), 876 (w), 772 (w), 743 (m), 632(w), and 571 (w).

2.2.4. $[Co_2(L^{tpbap})(3,5\text{-dbcat})_2](SO_4){\cdot}5.5MeOH{\cdot}2H_2O$ (**3a**)

To a solution of $CoSO_4{\cdot}7\ H_2O$ (56 mg, 0.2 mmol), we added **L^{tpbap}** (54 mg, 0.1 mmol) and **3,5-dbcat** (44 mg, 0.2 mmol) in 15 mL of methanol. Triethylamine (40 mg, 0.4 mmol) was added. The solution was heated under reflux for an hour. After cooling to room temperature, the solution was filtered and was allowed to evaporate slowly to yield green plates of complex **3a** suitable for X-ray diffraction. The crystals were obtained in high yields (83 mg, 0.07 mmol, 69.7%), separated by filtration and washed with cold methanol. Elemental Analysis: Found: C, 56.01; H, 7.75; N, 8.00; and S, 2.63. Calc. for $C_{60}H_{80}Co_2N_8O_8S{\cdot}5.5MeOH{\cdot}2H_2O$: C, 56.05; H, 7.61; N, 7.98; S, 2.28 %. IR (cm^{-1}) = 3415

(br), 2952 (m), 1612 (m), 1555 (w), 1463 (m), 1441 (m), 1413 (m),1359 (w), 1320 (w), 1281 (m), 1241 (m), 1120 (m), 979 (m), 826 (w), 769 (m), and 620 (m).

2.2.5. $[Co_2(L^{tpbap})(3,5\text{-dbcat})_2](ClO_4)_2 \cdot 1.5\ H_2O$ (**3b**)

To a solution of $Co(ClO_4)_2 \cdot 6H_2O$ (73 mg, 0.2 mmol), $\mathbf{L^{tpbap}}$ (54 mg, 0.1 mmol) and **3,5-dbcat** (44 mg, 0.2 mmol) in 15 mL of ethanol. Triethylamine (40 mg, 0.4 mmol) was added, and the reaction mixture was refluxed for an hour. After cooling to room temperature, the reaction solution was filtered and allowed to evaporate slowly. After a day, green crystals of complex **3b** were isolated by filtration in moderate yields (47 mg, 0.036 mmol, 36.3%) and washed with cold ethanol. Elemental Analysis: Found: C, 54.59; H, 6.13; N, and 8.45. Calc. for $C_{60}H_{80}Cl_2Co_2N_8O_{12} \cdot 1.5\ H_2O$: C, 54.55; H, 6.33; N, 8.48 %. IR (cm^{-1}) = 3424 (br), 2952 (m), 1611 (m), 1555 (w), 1461 (m), 1440 (m), 1413 (m),1359 (w), 1321 (w), 1281 (m), 1241 (m), 1204 (w), 1145 (m), 1118 (s), 1090 (s), 980 (m), 945 (w), 826 (w), 768 (m), and 626 (m).

Safety note: "Perchlorate complexes are potentially explosive. While we have not experienced any problems with the compounds described, they should be treated with caution and handled in small quantities".

3. Results and Discussion

The octadentate ligand 1,1′-(piperazine-1,4-diyl)bis(N,N-bis(pyridin-2ylmethyl)meth anamine) $\mathbf{L^{tpbap}}$ was synthesized in three steps (Scheme 1). Firstly, piperazine was cyanome thylated with chloroacetonitrile. Followed by reduction of the dinitriles to the corresponding diamine using lithium aluminium hydride. At the final step, a reductive amination of pyridine-2-carboxaldehyde was carried out to form $\mathbf{L^{tpbap}}$ in high yields. The ligand synthesized was characterized by ^{1}H-NMR, ^{13}C-NMR, and IR spectroscopy (Figures S1–S7).

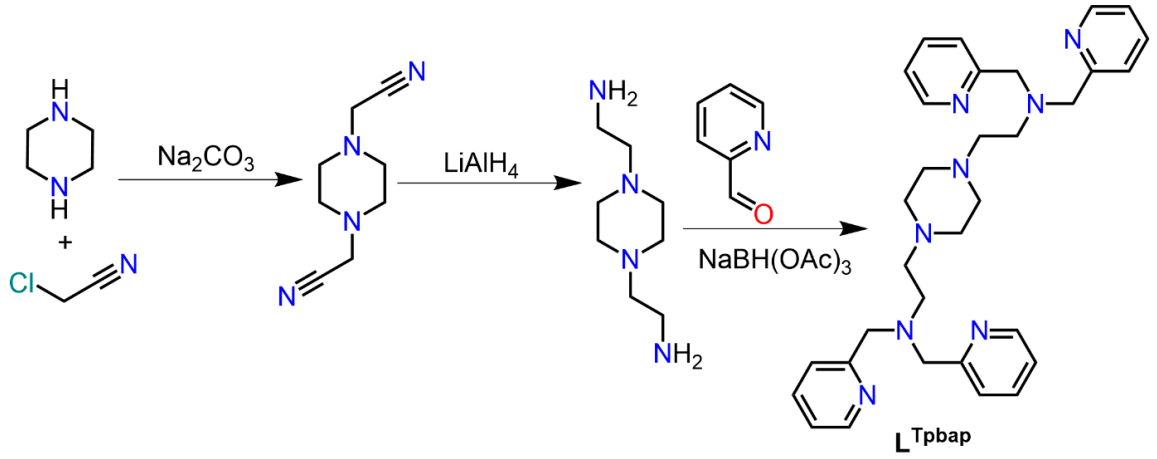

Scheme 1. Multistep ligand synthesis of octadentate ligand 1,1′-(piperazine-1,4-diyl)bis(N,N-bis(pyridin-2-ylmethyl)methanamine)($\mathbf{L^{tpbap}}$).

The mononuclear complexes were synthesized by reacting six equivalents of the commercially available 3,5-dbcat ligand with one equivalent of the cobalt precursor complex (P1) and the additional co-ligand 4-methylpiperdin to give [Co(**3,5-dbsq**)(**3,5-dbcat**)(4-Mepip)$_2$] (**1**), respectively, by reacting three equivalents of the commercially available tbcat with one equivalent of the precursor cobalt complex (P1) to give (Hpip)[Co(**tbcat**)$_2$(pip)$_2$]$\cdot CH_3CN$ (**2**).

In the case of the dinuclear complexes, the desired complexes were obtained by reacting one equivalence of the octadentate ligand $\mathbf{L^{tpbap}}$ with two equivalents of cobalt sulphate (**3a**) and cobalt perchlorate salt (**3b**) and two equivalents of **3,5-dbcat** in methanol in the case of **3a** and ethanol in the case of **3b**. Additionally, four equivalents of triethylamine were added as a base. The complexes $[Co_2(\mathbf{L^{tpbap}})(\mathbf{3,5\text{-}dbcat})_2](SO_4) \cdot 5.5MeOH \cdot 2H_2O$ (**3a**) and $[Co_2(\mathbf{L^{tpbap}})(\mathbf{3,5\text{-}dbcat})_2\ ](ClO_4)_2 \cdot 1.5\ H_2O$ (**3b**) were obtained as brown crystalline solid and washed with diethyl ether. The complexes obtained were characterized by elemental

analysis, X-ray diffraction at 173 K, infrared spectroscopy in the range of 450–3000 cm^{-1} (Figures S8–S11) and SQUID magnetometry in the temperature range of 2–380 K.

3.1. Crystal Structures

Brown needles of complex **1** crystallised from ethanolic solution after one day of slow evaporation. The X-ray data collected at 173 K shows that the compound crystallised in the non-centrosymmetric orthorhombic $Pca2_1$ ferroelectric space group as a desired mono-nuclear cobalt complex. The central metal ion is coordinated to two chelating 3,5-di-*tert*-butyldioxolene ligands along with two 4-methylpiperidines coordinated in *trans* position to each other as an ancillary co-ligand, as seen in Figure 1 and fully labelled complex **1** in Figure S13. Pierpont and co-workers have reported an analogue compound with pyridine as co-ligand [32]. The 4-methylpiperdine is more electron donating and stronger in ligand field strength compared to pyridine. In terms of the crystal geometry, the piperidine complex due to the chair conformation of the co-ligands exhibits lower symmetry. Moreover, the two hydrogen atoms at the 4-methylpiperidine N-atoms point to the same side of the complex the inversion symmetry at the central cobalt atom is broken. Both effects together have crucial influence on the non-equivalence of the electronic structure of the two coordinated dioxolene ligands. The coordination sphere around the cobalt metal ion with the bond distances of approximately 1.884 Å and 1.969 Å for Co-N and Co-O axis, respectively, clearly shows the presence of low spin Co(III) ion at the measuring temperature of 173 K, which was additionally confirmed by calculating the bond valence sum values (Table S3). The analysis of the intra-atomic distances of the ligands shows that the two dioxolene ligands are not equivalent. For one of the two ligands the alternating C-C bond length found within the ring and shorter C-O bond lengths of 1.302 Å for C1-O1 and 1.312 Å for C2-O2 clearly shows the existence of a partial double bond character (Table S1). In the case of the second dioxolene ligand longer C-O single bond distances are exhibited (1.348 Å and 1.362 Å for C15-O3 and C16-O4, respectively), as well as regular aromatic C-C bond length are seen. These bond distances help us to assign one dioxolene as a monoanionic semi-quinonate and the other one as an aromatic dianionic catecholate, which is also in agreement with the overall charge balance for the complex. VT at temperatures above 350 K will then lead to **1** being better described as $[Co^{II}(\mathbf{3,5\text{-}dbsq})_2(4\text{-Mepip})_2]$.

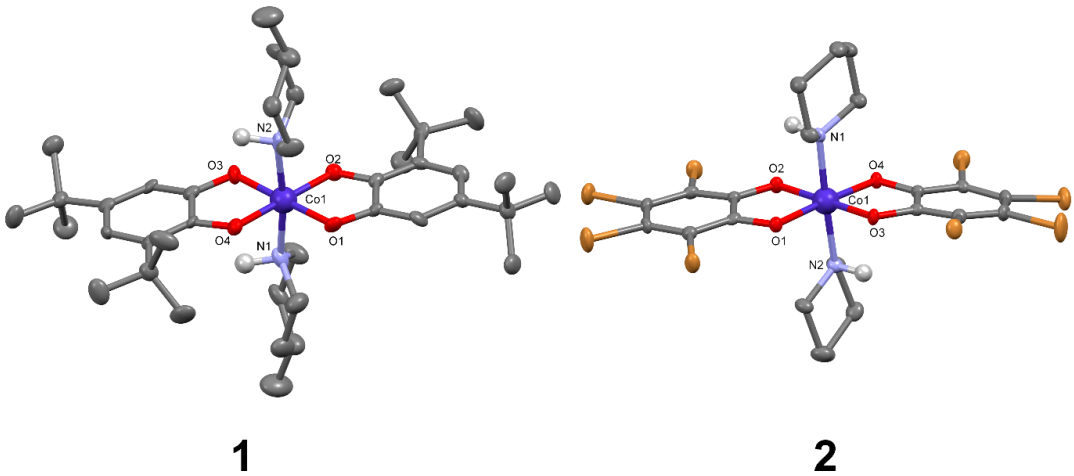

Figure 1. Crystal structures of $[Co(\mathbf{3,5\text{-}dbsq})(\mathbf{3,5\text{-}dbcat})(4\text{-Mepip})_2]$ (**1**) and $(Hpip)[Co(\mathbf{tbcat})_2(pip)_2]\cdot CH_3CN$ (**2**) collected at 173 K. The hydrogen atoms and lattice solvents are omitted for clarity. The 50% probability level for displacement ellipsoids.

Dark brown needles of complex **2** were obtained from slow evaporation of the complex from ethanolic solution. The X-ray data collected at 173 K shows that the compound crystalized in non-centrosymmetric monoclinic $P2_1$ ferroelectric space group as a desired mono-nuclear complex. The *tetra*-bromocatechol (**tbcat**) ligand used is a lot more electron

withdrawing compared to the **dbcat** ligand. The central metal ion coordination sphere is similar to that of the complex **1** with two dioxolene ligands coordinated to the cobalt ion along with the two piperidines co-ligand that are oriented in trans fashion. Interestingly, the hydrogen atoms of the coordinated nitrogen from the piperdine are orientated in the non-*meso* fashion, in contrast to complex **1** where the hydrogen atoms are oriented in the *meso* fashion, as seen in Figure 1 and fully labelled complex **2** in Figure S14. Complex **2** also consists of a piperidinium cation loosely bounded over hydrogen bridges to the oxygen atoms from the catecholate ligand with a bond distance of 2.771 Å and 2.819 Å. The bond distances as tabulated in Tables 1 and S2, indicate the presence of low spin Co(III) complex. The Bond Value Sum (BVS) calculated for the complex **2** for the cobalt^{3+} (Table S3) is slightly lower with a value of 2.8 compared to the other complexes at 173 K might be due to the electron withdrawing nature of the **tbcat** ligand.

Table 1. Selected bond length data for mono-nuclear complexes **1** and **2** and di-nuclear complexes **3a** and **3b** at 173 K.

Mono-Nuclear	**1**	**2**	**Di-Nuclear**	**3a**	**3b**
Metal-Donor	**Bond Length (Å)**	**Bond Length (Å)**	**Metal-Donor**	**Bond Length (Å)**	**Bond Length (Å)**
Co1-O1	1.901 (9)	1.909 (3)	Co1-O1	1.878 (4)	1.892 (6)
Co1-O2	1.905 (9)	1.901 (3)	Co1-O2	1.888 (4)	1.884 (5)
Co1-O3	1.885 (9)	1.907 (3)	Co1-N1	2.063 (5)	2.056 (5)
Co1-O4	1.884 (9)	1.893 (3)	Co1-N2	1.954 (4)	1.940 (6)
Co1-N1	1.969 (9)	2.014 (4)	Co1-N3	1.936 (5)	1.956 (6)
Co1-N2	1.978 (9)	2.019 (4)	Co1-N4	1.925 (5)	1.908 (7)

Thin green plates of di-nuclear isostructural complexes **3a** and **3b** were obtained in moderate yields from slow evaporation of a solution of ethanol. The X-ray data of the complexes was collected in both the cases at 173 K (Figure 2). Complex **3a** with a sulphate anion crystallizes in the monoclinic C2/c space group, whereas the complex **3b** with a perchlorate anion exhibits lower crystal symmetry and crystalizes in the triclinic, P-1 space group. In both the cases the cobalt–dioxolene fragments are oriented trans to each other. The metal donor distances of the cobalt ions in both complexes **3a** and **3b** show a strict undistorted octahedral coordination sphere with an average bond length of 1.85 Å and 1.95 Å for Co-O and Co-N, respectively. The bond lengths clearly indicate the presence of the low spin trivalent cobalt ions. The Bond Value Sum (BVS) calculated for the complex **3a** and **3b** (Table S3) for both cobalt 2+ and 3+ clearly indicate the presence of trivalent cobalt ions. The metal donor distances (Co-O and Co-N) at 173 K are tabulated in Table 1 and other crystallographic parameters in Table 2.

Table 2. Crystallographic data for mono-nuclear complexes **1** and **2** and di-nuclear complexes **3a** and **3b** collected at 173 K.

Compound	**1**	**2**
Empirical formula	$C_{40}H_{66}CoN_2O_4$	$C_{29}H_{37}Br_8CoN_4O_4$
Formula weight/g mol^{-1}	697.87	1203.83
Crystal size/mm	0.15 × 0.13 × 0.05	0.19 × 0.12 × 0.03
Crystal system	Orthorhombic	Monoclinic
Space group	*Pca2$_1$*	*P2$_1$*
CCDC No.	2202223	2195460
Unit cell dimensions		
a/Å	18.7294(3)	10.3888(2)
b/Å	10.7376(2)	17.3101(3)

Table 2. *Cont.*

c/Å	19.4878(4)	10.5887(2)
α/°	90	90
β/°	90	99.6854(9)
γ/°	90	90
Volume/Å	3919.2(14)	1877.04(6)
Z	4	2
$\rho_{calc.}$/g cm^{-1}	1.183	2.130
μ/mm^{-1}	0.478	9.012
F(000)	1516.0	1156.0
Temperature/K	173(2)	173(2)
Radiation	Mo-Kα	Mo-Kα
Index ranges	−22 < h < 20	−15 < h < 16
	−12 < k <12	−26 < k < 26
	−12 < l < 23	−16 < l < 15
Collected reflections	14473	54646
Independent reflections	5030	14399
R_{int}	0.1705	0.0673
R_{sigma}	0.2964	0.08060
Data/restraints/parameters	5030/105/439	14399/23/429
Goodness-of-fit on F^2	0.622	0.800
Final R_1 [$I \geq 2\sigma(I)$]	0.0469	0.0319
Final wR_2 [$I \geq 2\sigma(I)$]	0.0666	0.0496
Final R_1 [*alldata*]	0.1652	0.0577
Final wR_2 [*alldata*]	0.0961	0.0529
Compound	**3a**	**3b**
Empirical formula	$C_{69}H_{116}Co_2N_8O_{17}S$	$C_{60}H_{80}Cl_2Co_2N_8O_{12}$
Formula weight/g mol^{-1}	1479.61	1294.08
Crystal size/mm	0.46 × 0.34 × 0.3	0.19 × 0.15 × 0.02
Crystal system	Monoclinic	Triclinic
Space group	*C2/c*	$P\overline{1}$
CCDC No.	2170727	2170728
Unit cell dimensions		
a/Å	26.051(3)	11.071(2)
b/Å	17.448(2)	11.332(18)
c/Å	17.215(2)	15.543(3)
α/°	90	107.932(6)
β/°	94.177(3)	97.683(7)
γ/°	90	94.664(7)
Volume/Å	7804.4(18)	1823.1(5)
Z	4	1
$\rho_{calc.}$/g cm^{-1}	1.259	1.179
μ/mm^{-1}	0.519	0.585
F(000)	3168.0	680.0
Temperature/K	173(2)	173(2)
Radiation	Mo-Kα	Mo-Kα
Index ranges	−34 < h < 34	−13 < h < 14
	0 < k <22	−14 < k < 14
	0 < l < 22	−20 < l < 20
Collected reflections	13257	18429
Independent reflections	13257	8470
R_{int}	0.0207	0.1584
R_{sigma}	0.1309	0.3032
Data/ restraints/ parameters	13257/38/455	8740/79/379
Goodness-of-fit on F^2	1.041	0.941
Final R_1 [$I \geq 2\sigma(I)$]	0.0884	0.1072
Final wR_2 [$I \geq 2\sigma(I)$]	0.2066	0.2082
Final R_1 [*alldata*]	0.1786	0.2736
Final wR_2 [*alldata*]	0.2753	0.2692

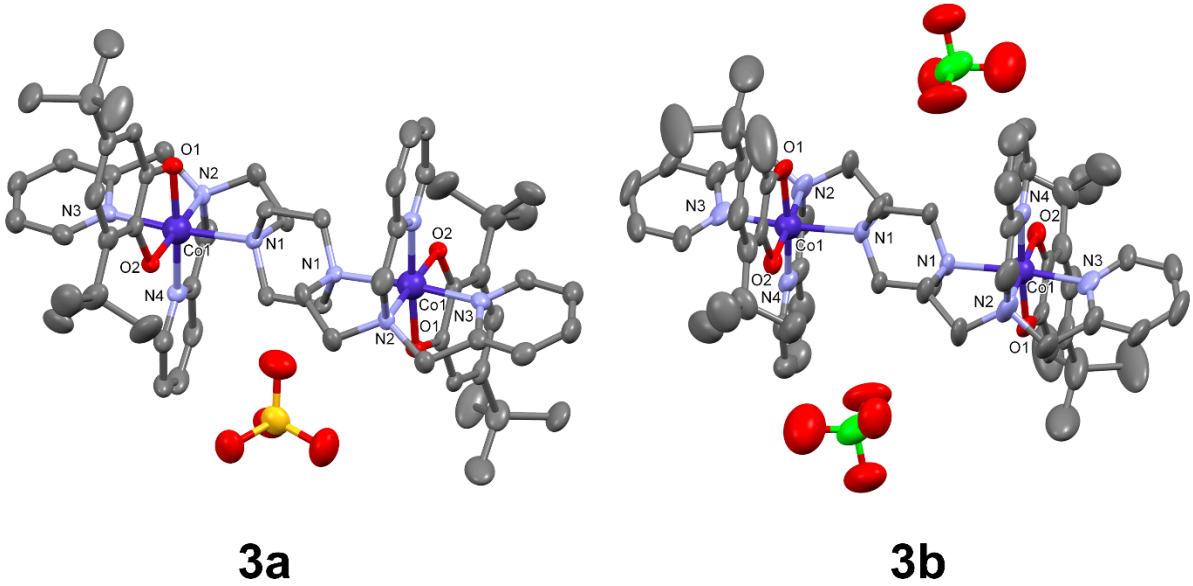

Figure 2. Complex structures of $[Co_2(\mathbf{L^{tpbap}})(\mathbf{3,5\text{-}dbcat})_2](SO_4)$ (**3a**) and $[Co_2(\mathbf{L^{tpbap}})(\mathbf{3,5\text{-}dbcat})_2](ClO_4)_2$ (**3b**) collected at 173 K. The hydrogen atoms and lattice solvents are omitted for clarity. The probability level for displacement ellipsoids is 50%.

It is evident from the literature that the VT conversion, accompanied with the spin transition from the low spin trivalent cobalt to a high spin divalent cobalt, the metal donor bond distances Co-O and Co-N are usually elongated by approximately 0.15 Å [22,24]. The crystalline lattice must be soft to enable the molecules to increase in volume in this way. In the case of **3b**, the molecules within the cell are aligned in the same way in the crystal structure. The crystal lattice exhibits only translational symmetry. Due to angularity and the interlocked arrangement a densely packed and rigid lattice environment is seen from crystal packing along the a–c plane as seen in Figure 3. The complex **3b** with the perchlorate anions does not show any hydrogen bonding but they exhibit a very weak π–π interaction between the pyridyl rings on the ligand backbone is observed. Thus, the rigid crystal lattice of complex **3b** hinders the expansion of the molecule which is usually seen with VT conversion. Interestingly, in the case of complex **3a**, a herringbone type packing pattern with an angle of 72.4° is found for the arrangement of $[Co_2(\mathbf{L^{tpbap}})(\mathbf{3,5\text{-}dbcat})_2]^{2+}$ cations. The packing is not symmetrical, and the molecules are not interlocked, as seen in the case of complex **3b**. The solvent methanol molecule and the sulphate anions are filled in the void spaces of the crystal packing. This also allows the molecule to have intermolecular interactions and cooperativity through extended hydrogen bonding network. As mentioned earlier, this enables the molecule to have a softer crystal lattice with flexibility to allow the expansion of the coordination sphere of the cobalt ion while exhibiting VT conversion. Similar impact of crystal packing, solvent incorporation and hydrogen bonding as lattice softening components is commonly reported for other mono-nuclear and di-nuclear cobalt dioxolene valence tautomers [25–27].

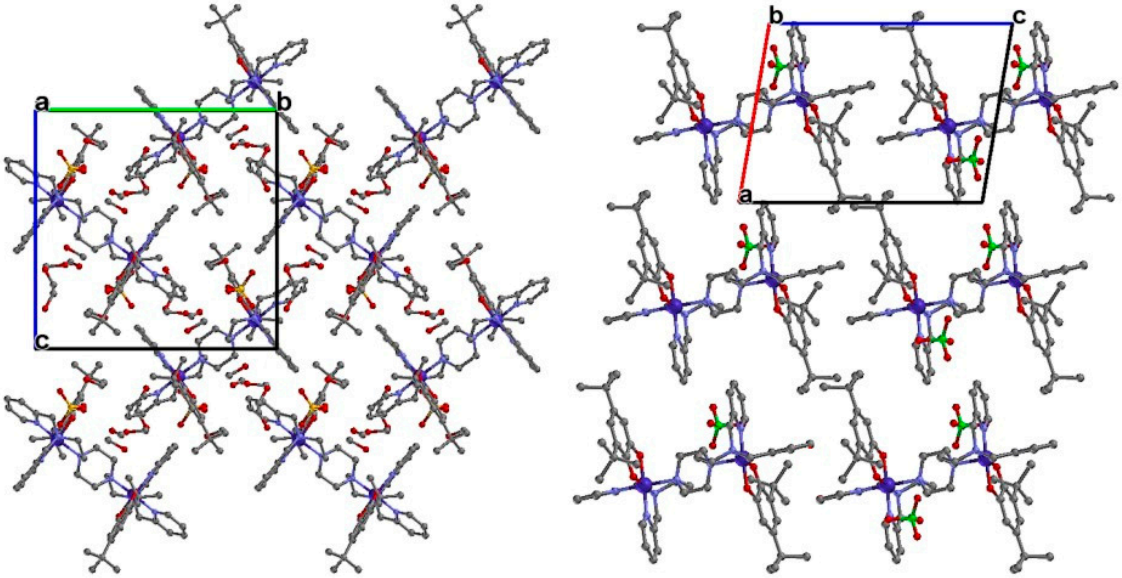

Figure 3. Difference in the crystal packing for **3a** and **3b**; Left: crystal packing of **3a** along the b–c plane and Right: crystal packing of **3b** along the a–c plane.

3.2. Magnetic Characterisation

Magnetic susceptibility data for all four complexes were measured on microcrystalline samples using a SQUID magnetometer in a temperature range from 2 K to 380 K, as shown in Figure 4. All four complexes show a low $\chi_M T$ values below room temperature, as anticipated for a trivalent cobalt diamagnetic ion, in agreement with the crystallographic data obtained at 173 K. For compound 1 only, X-ray structural analysis reveals one monoanionic semi-quinonate ligand, consistent with the overall charge balance of the complex, which leads to a finite value of 0.37 cm^3 K mol^{-1} at low temperature, fully consistent with an S = $\frac{1}{2}$ spin state for an uncoupled radical ligand. At temperatures above 300 K this value then increases to reach 0.51 cm^3 K mol^{-1} at 380 K. This small raise in the $\chi_M T$ value is assigned to a VT as further supported by the variable temperature solid state reflectance measurement carried over in the temperature range of 20 °C to 120 °C (S1212). The presence of the small amount of paramagnetic impurity is seen from the residual magnetic moment below room temperature. The mono-nuclear complex **1** shows a small increase in the $\chi_M T$ 0.36 cm^3 K mol^{-1} at 300 K to 0.51 cm^3 K mol^{-1} at 380 K. The small raise in the $\chi_M T$ value is further supported by the variable temperature solid state reflectance measurement carried out in the temperature range of 20 °C to 120 °C. At 20 °C for the Co^{III} (sq)(cat) species, the most prominent absorption bands are found at 244 nm, 310 nm, and 638 nm. By increasing the temperature, the intensity of the former and the latter decreases while new bands at 222 nm and 760 nm appear. This behaviour and the position of the absorption bands are in good agreement with the other thermochromic, valence tautomeric cobalt dioxolene complexes which also confirms the compound **1** exhibiting VT behaviour [32,33] (Figure S12). In the case of the di-nuclear complex with the sulphate anion **3a**, interestingly, above 300 K the magnetic moments show a sharp steady raise from a $\chi_M T$ value of 0.21 cm^3 K mol^{-1} at 300 K to 1.26 cm^3 K mol^{-1} at 380 K. This can be attributed to the VT interconversion to a cobalt(II) semi-quinonate along with a spin state transition to a high spin Co(II) species. The VT conversion in both the cases are incomplete within the measured temperature range. Literature evidence suggests that each uncoupled Co^{II}(sq) moiety will have a $\chi_M T$ value of 2.25 cm^3 K mol^{-1}. In the case of the complexes **2** and **3b** the magnetic moment remains unchanged over the measured temperature window which indicates VT interconversion does not exist over the measured temperature window because of the strong electron withdrawing nature of the **tbcat** ligand in the case of complex **2** and crystal packing effects in the case of complex **3b**.

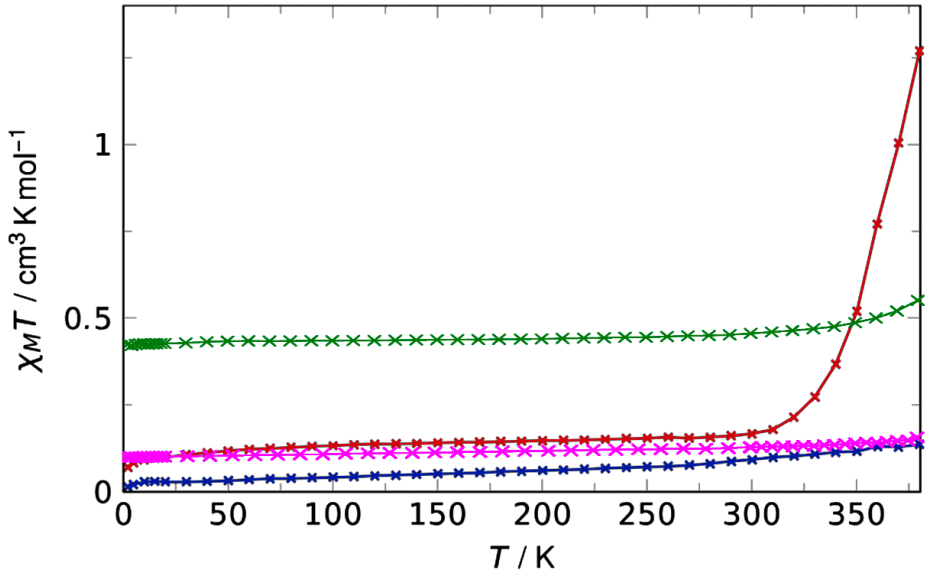

Figure 4. Magnetic susceptibility of complexes **1** (Green), **2** (Pink), **3a** (red) and **3b** (blue) measured from 2 to 380 K.

4. Conclusions

Herein, we reported the synthesis of a novel octadentate 1,1′-(piperazine-1,4-diyl)bis(N, N-bis(pyridin-2-ylmethyl)methanamine)(**L^{tpbap}**) ligand along with four novel cobalt complexes. [Co_2(**L^{tpbap}**)(**3,5-dbcat**)$_2$](SO_4)·5.5MeOH·2H_2O (**3a**) and [Co_2(**L^{tpbap}**)(**3,5-dbcat**)$_2$] (ClO_4)$_2$·1.5 H_2O (**3b**). The mono-nuclear complex **1**, [Co(3,5-dbsq)(**3,5-dbcat**)(4-Mepip)$_2$], and the di-nuclear complex **3a** show a gradual incomplete valance tautomerism around 300 K and 370K, respectively. In contrast, the complexes **2** and **3b** stay unchanged over the measured temperature window due to the effects of strong electron withdrawing ligand substituent on the catecholate in the case of complex **2** and crystal packing effects in solid state in the case of complex **3b**. Ongoing work is carried out to further fine-tune the ligand design by adding different substituents in the pyridine ring of the **L^{tpbap}** to study the electronic effects on achieving a complete VT in this ligand system.

Supplementary Materials: The following supporting information can be downloaded at: https://www.mdpi.com/article/10.3390/magnetochemistry8090109/s1, S1 ^{1}H-NMR Spectra: Figure S1: ^{1}H-NMR spectra of N,N′-Bis(cyanomethyl)piperazine; Figure S2: ^{1}H-NMR spectra of N,N′-Bis(2-aminoethyl)piperazine; Figure S3: ^{1}H-NMRspectraof1,1′-(piperazine-1,4-diyl)bis(N,Nbis(pyridinylm ethyl)methanamine)(**L^{tpbap}**) octadentate ligand. S2 ^{13}C-NMR Spectra: Figure S4: ^{13}C-NMR spectra of N,N′-Bis(cyanomethyl)piperazine; Figure S5: ^{13}C-NMR spectra of N,N′-Bis(2-aminoethyl)piperazine; Figure S6: ^{13}C-NMR spectra of N,N,N′,N′-Tetra-2-picolyl-1,4-bis(2-aminoethyl)piperazine (**L^{tpbap}**). S3 Infrared spectra: Figure S7: Infrared spectra of 1,1′-(piperazine-1,4-diyl)bis(N,Nbis(pyridinylmethyl) methanamine)(**L^{tpbap}**) octadentate ligand. Figure S8: Infrared spectra of ligand [Co(**3,5-dbsq**)(**3,5-dbcat**)$_2$(4-Mepip)$_2$] (**1**). Figure S9: Infrared spectra of ligand [Co(**tbcat**)$_2$(pip)$_2$] CH_3CN (**2**). Figure S10: Infrared spectra of ligand [Co_2(**L^{tpbap}**)(3,5-dbcat)$_2$](SO_4)·5.5MeOH·2H_2O (**3a**). Figure S11: Infrared spectra of ligand [Co_2 (**L^{tpbap}**)(3,5-dbcat)$_2$](ClO_4)2·1.5 H_2O (**3b**). Figure S12: Solid state reflectance spectra for complex **1**. The temperature dependence of the reflectance shows a VT- transition between 20 °C and 120 °C. Figure S13: Complex structure of **1** at 173 K with atom labels. Thermal displacement probability set to 50%; hydrogen atoms are omitted for clarity. Figure S14: Complex structure of **2** at 173 K with atom labels. Thermal displacement probability set to 50%; hydrogen atoms are omitted for clarity. S4 Bond length tables and crystal structures at 173 K: Table S1: Selected bond length for complex **1** at 173 K. Table S2: Selected bond length for complex **2** at 173 K. Table S3: Bond valence sum values (BVS) are calculated from literature known formula $Z_j = \Sigma S_{ij}$ tabulated extracted and calculated from the X-ray data obtained at 173 K for the Co ions in complex **1**,**2**, **3a** and **3b**.

Author Contributions: Conceptualization, E.R.; Data curation, L.M.C. and E.R.; Formal analysis, M.D. and L.M.C.; Investigation, S.S. and M.D.; Methodology, M.D.; Project administration, E.R.; Resources, E.R.; Supervision, E.R.; Validation, S.S. and L.M.C.; Visualization, S.S.; Writing—original draft, S.S. and M.D.; Writing—review & editing, S.S. and E.R. All authors have read and agreed to the published version of the manuscript.

Funding: The research was funded by Johannes Guttenberg University.

Institutional Review Board Statement: Not applicable.

Informed Consent Statement: Not applicable.

Data Availability Statement: The magnetic data presented in this study are available on request from the corresponding author.

Conflicts of Interest: The authors declare no conflict of interest.

References

1. Bousseksou, A.; Molnár, G.; Salmon, L.; Nicolazzi, W. Molecular spin crossover phenomenon: Recent achievements and prospects. *Chem. Soc. Rev.* **2011**, *40*, 3313–3335. [CrossRef]
2. Bousseksou, A.; Molnár, G.; Real, J.A.; Tanaka, K. Spin crossover and photomagnetism in dinuclear iron(II) compounds. *Coord. Chem. Rev.* **2007**, *251*, 1822–1833. [CrossRef]
3. Enriquez-Cabrera, A.; Rapakousiou, A.; Piedrahita Bello, M.; Molnár, G.; Salmon, L.; Bousseksou, A. Spin crossover polymer composites, polymers and related soft materials. *Coord. Chem. Rev.* **2020**, *419*, 213396. [CrossRef]
4. Gaspar, A.B.; Seredyuk, M. Spin crossover in soft matter. *Coord. Chem. Rev.* **2014**, *268*, 41–58. [CrossRef]
5. Atmani, C.; El Hajj, F.; Benmansour, S.; Marchivie, M.; Triki, S.; Conan, F.; Patinec, V.; Handel, H.; Dupouy, G.; Gómez-García, C.J. Guidelines to design new spin crossover materials. *Coord. Chem. Rev.* **2010**, *254*, 1559–1569. [CrossRef]
6. Sundaresan, S.; Eppelsheimer, J.; Carrella, L.M.; Rentschler, E. Three Novel Thiazole-Arm Containing 1, 3, 4-Oxadiazole-Based [HS-HS] Fe (II) Dinuclear Complexes. *Crystals* **2022**, *12*, 404. [CrossRef]
7. Halcrow, M.A. Structure:Function Relationships in Molecular Spin-Crossover Complexes. *Chem. Soc. Rev.* **2011**, *40*, 4119. [CrossRef]
8. Halcrow, M.A. (Ed.) *Spin-Crossover Materials: Properties and Applications*; John Wiley & Sons: Hoboken, NJ, USA, 2013; p. 568.
9. Hogue, R.W.; Singh, S.; Brooker, S. Spin crossover in discrete polynuclear iron(II) complexes. *Chem. Soc. Rev.* **2018**, *47*, 7303–7338 and inside front cover. [CrossRef]
10. Harding, D.J.; Harding, P.; Phonsri, W. Spin crossover in iron(III) complexes. *Coord. Chem. Rev.* **2016**, *313*, 38–61. [CrossRef]
11. Sundaresan, S.; Kitchen, J.A.; Brooker, S. Hydrophobic tail length in spin crossover active iron(II) complexes predictably tunes $T_{1/2}$ in solution and enables surface immobilization. *Inorg. Chem. Front.* **2020**, *7*, 2050–2059. [CrossRef]
12. Sundaresan, S.; Kühne, I.A.; Evesson, C.; Harris, M.M.; Fitzpatrick, A.J.; Ahmed, A.; Müller-Bunz, H.; Morgan, G.G. Compressed Jahn-Teller octahedra and spin quintet-triplet switching in coordinatively elastic manganese(III) complexes. *Polyhedron* **2021**, *208*, 115386. [CrossRef]
13. Boskovic, C. Valence Tautomeric Transitions in Cobalt-dioxolene Complexes. In *Spin-Crossover Materials: Properties and Applications*, 1st ed.; Halcrow, M.A., Ed.; John Wiley & Sons, Ltd.: Hoboken, NJ, USA, 2013; pp. 202–224.
14. Gütlich, P.; Dei, A. Valence Tautomeric Interconversion in Transition Metal 1,2-Benzoquinone Complexes. *Angew. Chem. Int. Ed.* **1997**, *36*, 2734–2736. [CrossRef]
15. Shaikh, N.; Goswami, S.; Panja, A.; Wang, X.-Y.; Gao, S.; Butcher, R.J.; Banerjee, P. New Route to the Mixed Valence Semiquinone-Catecholate Based Mononuclear FeIII and Catecholate Based Dinuclear MnIII Complexes: First Experimental Evidence of Valence Tautomerism in an Iron Complex. *Inorg. Chem.* **2004**, *43*, 5908–5918. [CrossRef] [PubMed]
16. Tao, J.; Maruyama, H.; Sato, O. Valence Tautomeric Transitions with Thermal Hysteresis around Room Temperature and Photoinduced Effects Observed in a Cobalt−Tetraoxolene Complex. *J. Am. Chem. Soc.* **2006**, *128*, 1790–1791. [CrossRef]
17. Tezgerevska, T.; Alley, K.G.; Boskovic, C. Valence tautomerism in metal complexes: Stimulated and reversible intramolecular electron transfer between metal centers and organic ligands. *Coord. Chem. Rev.* **2014**, *268*, 23–40. [CrossRef]
18. Affronte, M.; Beni, A.; Dei, A.; Sorace, L. Valence Tautomerism Interconversion Triggers Transition to Stable Charge Distribution in Solid Polymeric Cobalt-polyoxolene Complexes. *Dalton Trans.* **2007**, *45*, 5253–5259. [CrossRef]
19. Dapporto, P.; Dei, A.; Poneti, G.; Sorace, L. Complete Direct and Reverse Optically Induced Valence Tautomeric Interconversion in a Cobalt–Dioxolene Complex. *Chem. Eur. J.* **2008**, *14*, 10915–10918. [CrossRef]
20. Nadurata, V.L.; Hay, M.A.; Janetzki, J.T.; Gransbury, G.K.; Boskovic, C. Rich redox-activity and solvatochromism in a family of heteroleptic cobalt complexes. *Dalton Trans.* **2021**, *50*, 16631–16646. [CrossRef]
21. Poneti, G.; Mannini, M.; Sorace, L.; Sainctavit, P.; Arrio, M.-A.; Otero, E.; Criginski Cezar, J.; Dei, A. Soft-X-ray-Induced Redox Isomerism in a Cobalt Dioxolene Complex. *Angew. Chem. Int. Ed.* **2010**, *49*, 1954–1957. [CrossRef]
22. Alley, K.G.; Poneti, G.; Aitken, J.B.; Hocking, R.K.; Moubaraki, B.; Murray, K.S.; Abrahams, B.F.; Harris, H.H.; Sorace, L.; Boskovic, C. A Two-Step Valence Tautomeric Transition in a Dinuclear Cobalt Complex. *Inorg. Chem.* **2012**, *51*, 3944–3946. [CrossRef]

23. Alley, K.G.; Poneti, G.; Robinson, P.S.D.; Nafady, A.; Moubaraki, B.; Aitken, J.B.; Drew, S.C.; Ritchie, C.; Abrahams, B.F.; Hocking, R.K.; et al. Redox Activity and Two-Step Valence Tautomerism in a Family of Dinuclear Cobalt Complexes with a Spiroconjugated Bis(dioxolene) Ligand. *J. Am. Chem. Soc.* **2013**, *135*, 8304–8323. [CrossRef]
24. Evangelio, E.; Ruiz-Molina, D. Valence Tautomerism: New Challenges for Electroactive Ligands. *Eur. J. Inorg. Chem.* **2005**, *2005*, 2957–2971. [CrossRef]
25. Sheldrick, G.M. *SHELXTL-Plus. Graphical Interface for Crystal Structure Solution and Refinement*; Bruker Analytical X-ray Instruments Inc.: Madison, WI, USA, 1998.
26. Sheldrick, G.M. SHELXT—Integrated space-group and crystal-structure determination. *Acta Crystallogr. Sect. A* **2015**, *71*, 3–8. [CrossRef]
27. Sheldrick, G. A short history of SHELX. *Acta Cryst. A* **2008**, *64*, 112–122. [CrossRef]
28. Sheldrick, G.M. Crystal structure refinement with SHELXL. *Acta Crystallogr. Sect. C* **2015**, *71*, 3–8. [CrossRef]
29. Dolomanov, O.V.; Bourhis, L.J.; Gildea, R.J.; Howard, J.A.K.; Puschmann, H. OLEX2: A complete structure solution, refinement and analysis program. *J. Appl. Cryst.* **2009**, *42*, 339–341. [CrossRef]
30. O'Connor, C.J. Magnetochemistry—Advances in Theory and Experimentation. *Prog. Inorg. Chem.* **1982**, *29*, 203–283.
31. Aromí, G.; Batsanov, A.S.; Christian, P.; Helliwell, M.; Parkin, A.; Parsons, S.; Smith, A.A.; Timco, G.A.; Winpenny, R.E.P. Synthetic and Structural Studies of Cobalt–Pivalate Complexes. *Chem. Eur. J.* **2003**, *9*, 5142–5161. [CrossRef]
32. Jung, O.-S.; Jo, D.H.; Lee, Y.-A.; Conklin, B.J.; Pierpont, C.G. Bistability and Molecular Switching for Semiquinone and Catechol Complexes of Cobalt. Studies on Redox Isomerism for the Bis(pyridine) Ether Series Co(py2X)(3,6-DBQ)2, X = O, S, Se, and Te. *Inorg. Chem.* **1997**, *36*, 19–24. [CrossRef]
33. Liang, H.; Na, M.Y.; Chun, S.I.; Kwon, S.S.; Lee, Y.-A.; Jung, O.-S. Dinuclear Valence Tautomeric 1,2-Semiquinonato/Catecholatocobalt Complexes Containing 1,1,4,7,10,10-Hexamethyltriethylenetetramine. *Bull. Chem. Soc. Jpn.* **2007**, *80*, 916–921. [CrossRef]